Numerical investigation of electron trajectories in the Columbia Non-neutral Torus

Benoit Durand de Gevigney, Thomas Sunn Pedersen, and Allen H. Boozer
Department of Applied Physics and Applied Mathematics, Columbia University, New York 10027, USA

(Received 9 September 2009; accepted 5 October 2009; published online 3 December 2009)

The confinement of pure electron plasmas in the Columbia Non-neutral Torus (CNT) [T. Sunn Pedersen *et al.*, Fusion Sci. Technol. **50**, 372 (2006)] can be enhanced by the large radial electric field due to space charge. However the benefits are limited by two effects: (1) The $\vec{E}\times\vec{B}$ precession can, at low B-fields, resonate with the particle motion along the magnetic field lines, which gives large excursions in the trajectories. (2) Variations in the electric potential on magnetic surfaces, inherent to CNT equilibrium, add to the complexity of the trajectories and can also lead to large excursions. The second effect is sensitive to the conductive structures outside the plasma boundary. Results from a new code to investigate electron trajectories in the magnetic and electric field expected in CNT are presented. © *2009 American Institute of Physics*. [doi:10.1063/1.3259967]

I. INTRODUCTION

Non-neutral plasmas are traditionally confined in Penning–Malmberg traps which are open field-line devices.[1] Symmetries in the cylindrical geometry imply excellent confinement properties.[2] Even very limited breaking of this symmetry in either the magnetic[3] or the electric field[4] has been shown to cause transport via trapped-particle modes.[5,6] The "rotating wall technique" counteracts the drag caused by asymmetries using an external electric field rotating with the plasma[7,8] and allows for essentially arbitrary long confinement times. The self-electric field produced by charge imbalance in a non-neutral plasma also has a crucial influence on particle orbits[9] and on the dynamics of the plasma. This electric field is essential for trapping non-neutral plasmas in pure toroidal field machines as it provides the poloidal rotation necessary to close the drift orbits.[10,11] Recent experimental progress in this type of device led to confinement times approaching the theoretical limit set by magnetic pumping transport.[12,13] Trapping of non-neutral plasmas on magnetic surfaces relies on the rotational transform to close the orbits of magnetically passing particles whereas magnetically trapped particles are confined by the strong radial electric field. Confinement is theoretically limited by neoclassical transport.[14]

The Columbia Non-neutral Torus (CNT) is a simple stellarator made of only four planar coils and dedicated to the study of plasmas of arbitrary neutrality confined on magnetic surfaces.[15,16] This is not an optimized stellarator and it exhibits large variations in magnetic field strength on surfaces but particle confinement is expected to be good because of the large radial electric field.[14,17] Nevertheless the observed neoclassical confinement time is orders of magnitude less than the predicted confinement time.[18] Investigation of electron trajectories in pure electron plasmas, which is the subject of this paper, sheds some light on the reasons for this discrepancy.

For pure electron plasmas confined on magnetic surfaces, the electric potential Φ is dictated by a Poisson–Boltzmann equation,[14]

$$\nabla^2\Phi = \frac{e}{\epsilon_0}N(\psi)\exp\left(\frac{e\Phi}{T_e(\psi)}\right). \tag{1}$$

Here ψ is a label for magnetic surfaces and $N(\psi)$ determines the average electron density on each ψ surface. The electron temperature $T_e(\psi)$ is assumed constant on each magnetic surface and is typically 4 eV in CNT. A three-dimensional (3D) code was developed which solves Eq. (1) in the nontrivial geometry of CNT.[19] This code shows that the potential varies significantly on magnetic surfaces when there are few Debye lengths in the plasma ($a \lesssim \lambda_D$) but tends to be constant on surfaces when many Debye lengths are present ($a \gtrsim 10\lambda_D$). However the equilibria are quite sensitive to electrostatic boundary conditions. In CNT, in the absence of the good conductor surrounding the plasma that was recently installed, and even for $\lambda_D = 1.5$ cm $\ll a \simeq 15$ cm, potential variations on the outer surfaces are significant.

Because of the electron space charge, all equilibria exhibit very strong, negative electric fields ($e|\Delta\Phi|/T_e \gg 1$). The beneficial influence of a moderate ambipolar electric field on the confinement of quasineutral plasmas in stellarators is well established.[20,21] This paper investigates the effects of very strong electric fields on confinement. It is shown that a purely radial electric field greatly improves the quality of the trajectories, as expected. However because the electric field is so strong toroidal resonances appear at moderately low values of the magnetic field leading to unconfined orbits. In addition, potential variations on surfaces add to the complexity and the possibility of unconfined trajectories.

II. ELECTRON TRAJECTORIES

A. Boozer flux coordinates

We make use of Boozer flux coordinates (ψ, θ, φ).[22] ψ is a radial coordinate proportional to the toroidal magnetic flux and $\psi = \psi_b$ at plasma boundary. θ and φ are poloidal and toroidal angles, respectively. In this system of coordinates,

$$\vec{B} = \vec{\nabla}\psi \times \vec{\nabla}\theta + \iota(\psi)\vec{\nabla}\varphi \times \vec{\nabla}\psi,$$

$$= (\mu_0 G/2\pi)\vec{\nabla}\varphi, \tag{2}$$

where G is the current in the interlocking coils. The first equation holds whenever magnetic surfaces exist. The second one implies $\vec{B}$ is curl-free which holds in CNT since the plasma current density is totally negligible (see Ref. 14) so the magnetic field is just the field due to the coils. In the (φ,θ)-plane field lines are straight with a slope $\iota(\psi)$, the rotational transform (the average number of poloidal circuits a magnetic field line makes per toroidal circuit). These coordinates are derived in CNT using simple integration along the field lines, as described in Ref. 23.

There are many advantages of using Boozer coordinates. One of these is that the drift motion depends only on the magnetic field strength and not on its direction. CNT has twofold periodicity and stellarator symmetry about the point $(\theta,\varphi)=(0,0)$ meaning that the magnetic field strength can be described as $B=\Sigma b_{mn}\cos(m\theta-2n\varphi)$. The $n=0$ components of B are the toroidal components, whereas the $n\neq 0$ are the helical components. For an accurate description of the magnetic field we keep about 60 terms in this Fourier series. A magnetic field strength of 0.1 T is typical of CNT and will be used in this paper, unless otherwise stated.

The equations of motion in Boozer coordinates take a very simple Hamiltonian form.[24] Introducing $\theta_0 \equiv \theta - \iota\varphi$, $\chi \equiv (\mu_0 G/2\pi)\varphi$, $\rho_\parallel \equiv m v_\parallel / eB$, and $\mu \equiv m v_\perp^2 / 2B$ the conserved magnetic moment, the drift equations take the form

$$\frac{d\psi}{dt} = -\frac{\partial\Phi}{\partial\theta_0} + \left(\frac{eB}{m}\rho_\parallel^2 + \frac{\mu}{e}\right)\frac{\partial B}{\partial\theta_0}, \tag{3}$$

$$\frac{d\theta_0}{dt} = \frac{\partial\Phi}{\partial\psi} - \left(\frac{eB}{m}\rho_\parallel^2 + \frac{\mu}{e}\right)\frac{\partial B}{\partial\psi}, \tag{4}$$

$$\frac{d\chi}{dt} = \frac{eB^2}{m}\rho_\parallel, \tag{5}$$

$$\frac{d\rho_\parallel}{dt} = \frac{\partial\Phi}{\partial\chi} - \left(\frac{eB}{m}\rho_\parallel^2 + \frac{\mu}{e}\right)\frac{\partial B}{\partial\chi}. \tag{6}$$

Because of the very complicated magnetic field structure and the potentially complicated electric field, not necessarily constant on surfaces, we decided to investigate electron trajectories numerically. The equations of motion are integrated in time by a fourth-order Runge–Kutta integrator, adjusting the step size so as to conserve total energy with a certain tolerance. Analytical estimates are given when possible.

B. Choice of electric potential

We will focus our attention on three different electrostatic potentials. In Sec. III, we investigate the electron trajectories in the absence of an electric field, $\Phi=0$. This represents the situation where there is negligible space charge, and serves to illustrate the quality of the trajectories given

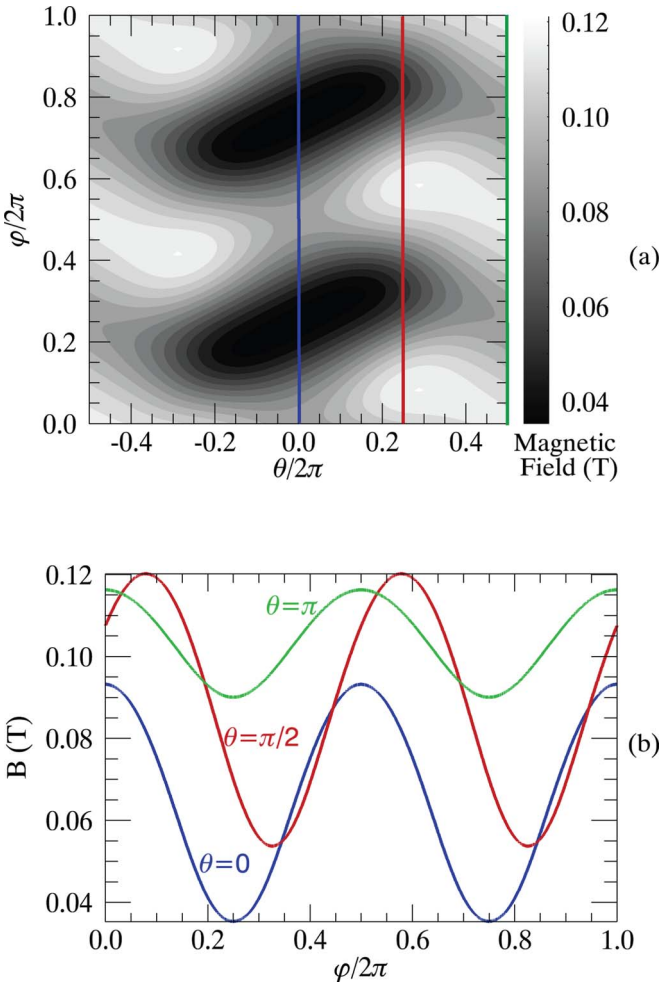

FIG. 1. (Color online) (a) Map of B on the surface $\psi=0.5\psi_b$. (b) Plot of B along lines of constant θ. One clearly distinguishes the large helical variations in B and the two troughs centered around $\theta=0$. $\theta=0$ corresponds to the outside (low B-field region) board of the torus whereas $\theta=\pm\pi$ corresponds to the inside (high B-field) board of the torus.

the magnetic topology without electrostatic (primarily $\vec{E}\times\vec{B}$) effects. In Sec. IV, we investigate the trajectories in the case of a strong electric potential, constant on the magnetic surfaces. This is an idealized situation which should lead to vastly improved confinement. In Sec. V, we investigate an electrostatic potential that has significant variations on the magnetic surfaces. The potential chosen is a reasonably accurate representation of the actual electrostatic potential in CNT, and gives rise to complicated drift trajectories.

III. NO ELECTRIC POTENTIAL

As mentioned above, CNT has a very simple coil configuration. Thus its magnetic topology is very different from those of highly optimized stellarators such as W7-X.[25] In particular there are huge variations in B on surfaces, see Fig. 1.

Because of these large variations in B there exists a very large fraction of trapped electrons, mostly helically trapped. Because these electrons are trapped in magnetic wells, they cannot take advantage of the ι-induced poloidal rotation.

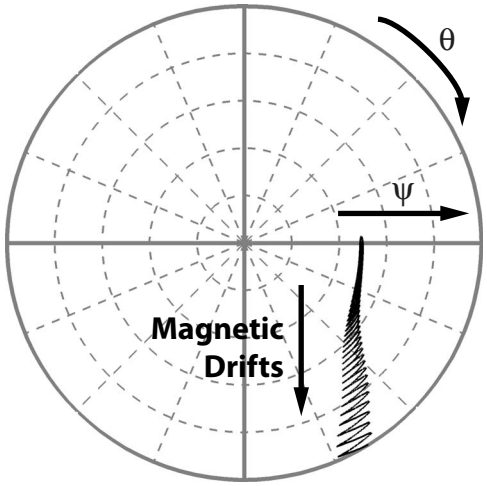

FIG. 2. Trajectory of an electron in the absence of electric field. The electron, born at a minimum of B, is helically trapped and quickly lost.

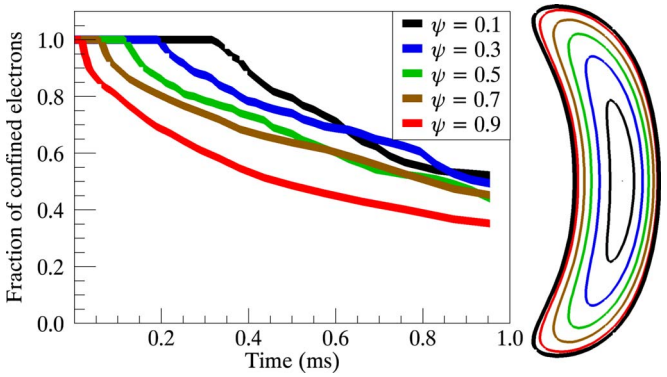

FIG. 4. (Color online) Fraction of confined electrons vs time on different surfaces in the absence of electric field. 1000 4 eV electrons are initially started on each surface. On the right are the corresponding surfaces seen on a cross section of the plasma.

These trapped electrons stay localized in the poloidal direction and magnetically drift out of the torus on a characteristic time scale of

$$t_{\text{loss}} = \frac{a}{v_D} \simeq \frac{eaRB}{mv^2}, \tag{7}$$

where a is the minor radius and R is the major radius. In CNT, $a \simeq 13$ cm and $R \simeq 22$ cm. So for a $W_k = 4$ eV electron in a $B = 0.1$ T magnetic field, this estimate yields $t_{\text{loss}} \simeq 0.4$ ms. The typical trajectory of a helically trapped electron is given in Figs. 2 and 3.

Because there is a large fraction of trapped electrons we expect direct losses to be large. Moreover because all surfaces are subject to variations in B, all surfaces have a potentially large loss cone. To assess the confinement of single trajectories, 1000 electrons are started on a ψ-surface and followed until they leave the confinement region. The electrons are sampled with random poloidal angle, toroidal angle, and pitch, but all have kinetic energy $W_k = 4$ eV. In Fig. 4 we plot the fraction of confined electrons as a function of time and for electrons starting on different surfaces. We can observe that even deep in the plasma more than half of the electrons are lost.

An electron born with a pitch $\lambda = v_{\parallel}/v$ at a location (ψ, θ, φ) is magnetically trapped on its birth surface if

$$|\lambda| \leq \lambda_{\max}(\psi, \theta, \varphi) \equiv \sqrt{1 - \frac{B(\psi, \theta, \varphi)}{B_{\max}(\psi)}}, \tag{8}$$

where $B_{\max}(\psi)$ is the maximum of the B-field on the surface ψ. Similarly, the electron can be trapped by local *helical* variations in B, with a local maximum B_{hel}. The electron is then *helically* trapped if

$$|\lambda| \leq \lambda_{\text{hel}}(\psi, \theta, \varphi) \equiv \sqrt{1 - \frac{B(\psi, \theta, \varphi)}{B_{\text{hel}}}}. \tag{9}$$

Because $B_{\text{hel}} \leq B_{\max}$, $\lambda_{\text{hel}} \leq \lambda_{\max}$, and there are electrons with a pitch close enough to $\lambda_{\max}$ which are only toroidally trapped, not helically trapped. Toroidally trapped electrons, although lost in general, are lost less quickly than helically trapped electrons. This is illustrated in Fig. 5.

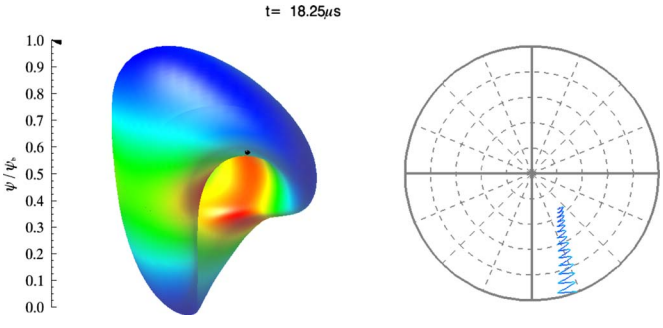

FIG. 3. (Color online) Trajectory of a helically trapped electron in the absence of electric field. On the left hand side is a vertical scale giving ψ/ψ_b, the normalized radial position of the electron. In the middle is a 3D view of the electron on its magnetic surface. The surface is colored according to the magnitude of $\vec{B}$ on this surface, red being high B, yellow-green being mild B, and blue being low B. On the right hand side is the trajectory of the electron projected onto the (ψ, θ) plane as in Fig. 2 (enhanced online).[URL: http://dx.doi.org/10.1063/1.3259967.1]

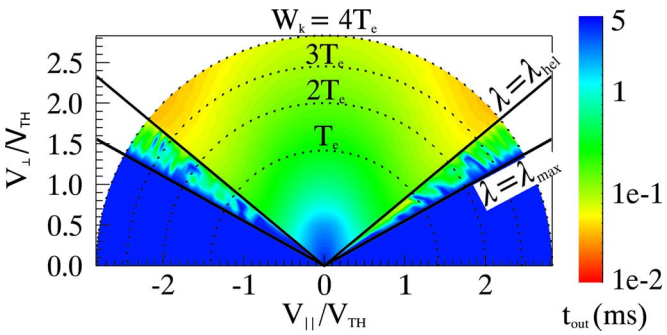

FIG. 5. (Color online) Loss cone structure in the absence of electric field at a minimum of B on the surface $\psi = 0.9\psi_b$. t_{out} denotes the time it takes an electron to leave confinement. A 5 ms confinement time is considered infinite confinement time. One can clearly distinguish the region of helical trapping, $|\lambda| \leq |\lambda_{\text{hel}}|$, from the region of toroidal trapping $|\lambda_{\text{hel}}| \leq |\lambda| \leq |\lambda_{\max}|$.

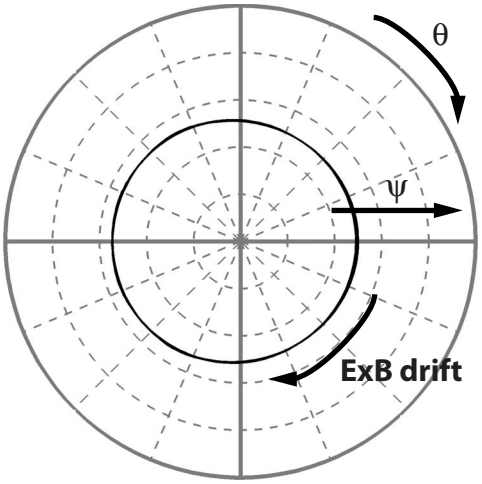

FIG. 6. Orbit of a helically trapped electron in a strong, purely radial electric field. The electron stays helically trapped but the $\vec{E}\times\vec{B}$ drift effectively closes the orbit in the poloidal direction.

IV. ELECTRIC POTENTIAL CONSTANT ON SURFACES, $\Phi(\psi)$

A. Orbits' confinement

Having a potential constant on surfaces adds a purely poloidal $\vec{E}\times\vec{B}$-drift component to the equation of motion, Eq. (4). Because the electric field is negative this poloidal rotation is in the positive θ direction. The poloidal rotation induced by the rotational transform depends on $v_\parallel$. So the $\vec{E}\times\vec{B}$ drift motion and the motion of electrons along field lines are added to calculate $d\theta/dt$ when $v_\parallel>0$ but subtract from each other when $v_\parallel<0$. However, for ι to provide poloidal rotation, the electron has to travel along the field lines, whereas the $\vec{E}\times\vec{B}$ rotation is also effective for trapped electrons. Hence the $\vec{E}\times\vec{B}$ drift can help to close the orbits of trapped electrons. As an illustration we give in Fig. 6 (Fig. 7) the orbit of the same helically trapped electron as in Fig. 2 (Fig. 3), this time with a strong radial electric field.

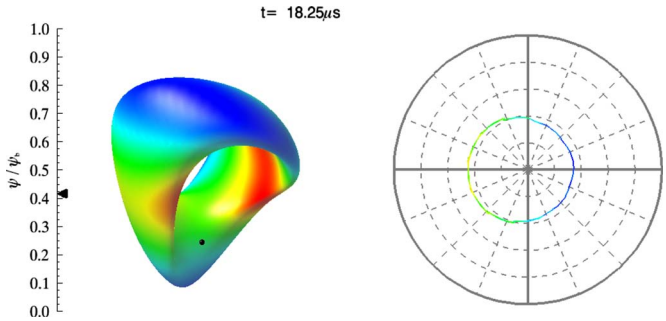

FIG. 7. (Color online) Trajectory of a helically trapped electron in a strong and purely radial electric field. On the left hand side is a vertical scale giving ψ/ψ_b, the normalized radial position of the electron. In the middle is a 3D view of the electron on its magnetic surface. The surface is colored according to the magnitude of $\vec{B}$ on this surface, red being high B, yellow-green being mild B, and blue being low B. On the right hand side is the trajectory of the electron projected onto the (ψ,θ) plane as in Fig. 6 (enhanced online).[URL: http://dx.doi.org/10.1063/1.3259967.2]

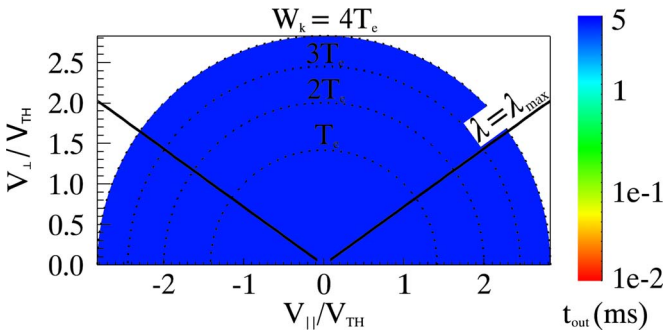

FIG. 8. (Color online) Loss cone structure in the case of a strong, purely radial electric field at a minimum of B on the surface $\psi=0.5\psi_b$. t_{out} denotes the time it takes an electron to leave confinement. A 5 ms confinement time is considered infinite confinement time. All trapped electrons are perfectly confined by the $\vec{E}\times\vec{B}$-rotation—compare with Fig. 5.

This process is effective if t_{loss}, the typical loss time of an electron, is long compared to $t_{\vec{E}\times\vec{B}}$, the half-poloidal transit time due to the $\vec{E}\times\vec{B}$ drift,

$$t_{\vec{E}\times\vec{B}}=\frac{\pi a}{v_{\vec{E}\times\vec{B}}}=\frac{\pi a^2 B}{\Delta\Phi}. \tag{10}$$

As mentioned earlier, in CNT $e\Delta\Phi\gg T_e$ so that for a thermal electron

$$\frac{t_{\vec{E}\times\vec{B}}}{t_{\text{loss}}}=\left(\frac{2\pi a}{R}\right)\frac{W_k}{e\Delta\Phi}\ll 1 \tag{11}$$

and closing of the orbits through $\vec{E}\times\vec{B}$ drift is very effective. This is illustrated in Fig. 8 where we plot the loss cone at a minimum of the B-field on the surface $\psi=0.5\psi_b$.

B. Direct losses

Only electrons that have enough kinetic energy and that are born close enough to the plasma boundary can escape confinement before closing their orbits in the poloidal direction. Consider a deeply helically trapped electron, $\lambda\simeq 0$, $\varphi=\varphi_i\simeq$ const born at low B-field, B_i, on the surface $\psi=\psi_i$ with kinetic energy $W_{k,i}$. The worst case is if the electron is born with $\theta=0$ so that it has to make a complete half poloidal rotation before the magnetic drifts become favorable. Assuming the electron stays helically trapped during its motion and using Eq. (3)–(5),

$$\frac{d\psi}{dt}\simeq\frac{\mu}{e}\frac{\partial B}{\partial\theta}\quad\text{and}\quad\frac{d\theta}{dt}\simeq\Phi'\equiv\frac{d\Phi}{d\psi}. \tag{12}$$

So that along the motion of this electron and averaged over a bounce period,

$$\Delta\psi=\frac{\mu}{e}\int d\theta\frac{\partial_\theta B}{\Phi'}. \tag{13}$$

The electron is confined if

$$\frac{\mu}{e}\int_0^\pi d\theta\frac{\partial_\theta B}{\Phi'}\le\psi_b-\psi_i. \tag{14}$$

Estimating

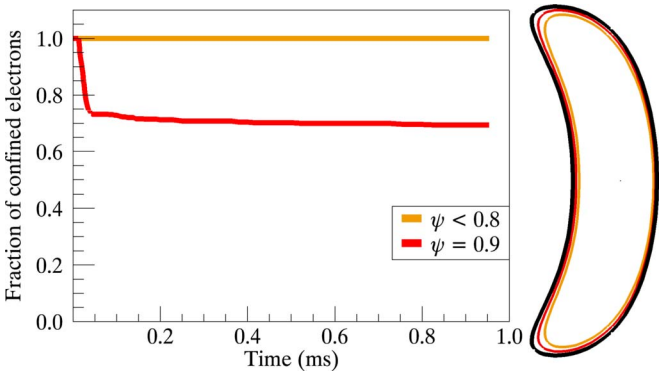

FIG. 9. (Color online) Fraction of confined electrons vs time on different surfaces in the case of a strong and purely radial electric field. 1000 4 eV electrons are initially started on each surface. Only electrons born very close to the last closed surface are lost.

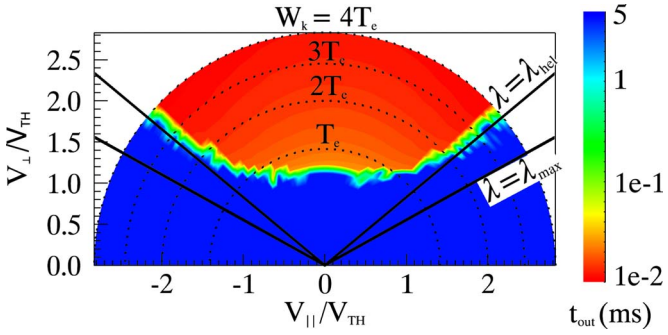

FIG. 10. (Color online) Loss cone structure in the case of a strong, purely radial electric field at a minimum of B on the surface $\psi=0.9\psi_b$. t_{out} denotes the time it takes an electron to leave confinement. A 5 ms confinement time is considered infinite confinement time. Only high energy helically trapped electrons are lost.

$$\Phi' \sim \frac{\int_{\psi_i}^{\psi_b} d\psi \Phi'}{\psi_b - \psi_i} = \frac{\Delta\Phi(\psi_i)}{\psi_b - \psi_i} \tag{15}$$

with

$$\Delta\Phi(\psi_i) = \Phi(\psi_b) - \Phi(\psi_i) \tag{16}$$

and making use of $\mu = W_{k,i}/B_i$, the electron is confined if

$$\left(\frac{B(\psi=\psi_b,\ \theta=\pi,\ \varphi=\varphi_i)}{B(\psi=\psi_i,\ \theta=0,\ \varphi=\varphi_i)} - 1 \right) \lesssim \frac{e\Delta\Phi(\psi_i)}{W_{k,i}}. \tag{17}$$

This estimate allows us to find on which surface electrons with a given initial kinetic energy will begin to be lost. For example, for the potential we use, 4 eV electrons can be lost only if born with $\psi \gtrsim 0.85\psi_b$. The electric field indeed greatly increases the confinement of orbits. This is confirmed numerically by running a simulation similar to the one presented in previous section where we start 1000 4 eV electrons on different ψ-surfaces and keep track of the fraction of confined electrons in time. The initial phase space sampling is as described before. Results are presented in Fig. 9.

Because a potential that is constant on surfaces does not trap electrons electrostatically, the loss cone with such a potential is somewhat similar to the one without potential. The main difference is that electrons need a kinetic above a certain threshold, given by Eq. (17), to be lost, see Fig. 10.

The separatrix $W_k^{sep}(\lambda)$ between lost and confined orbits is plotted more precisely in Fig. 11. Its details can be understood by noticing that there are very large variations in B along the toroidal line $\theta=0$ whereas variations in B along the line $\theta=\pi$ are much shallower—see Fig. 1. Thus an electron trapped at the minimum of B at $\theta=0$ is not necessarily trapped at $\theta=\pi$ provided it has a sufficiently high initial pitch.

An electron born at $\theta=0$ with a very small pitch, see Fig. 12(a), is and stays helically trapped however shallow the magnetic well is at $\theta=\pi$. That is, an electron with a very small initial pitch stays helically trapped during all of its poloidal motion. Such an electron is lost if its initial kinetic energy is above the threshold given by Eq. (17). This accounts for the flat region $|\lambda| \lesssim 0.25$ in Fig. 11. An electron born with a higher initial pitch, as in Figs. 12(b) and 12(c), has enough initial parallel kinetic energy to leave the helical trap during its poloidal motion. It does not complete a full poloidal period being helically trapped in the same trap. As it has more freedom to move poloidally around the torus, it has more chances to average out its radial drift. This electron can thus be born with a kinetic energy above the threshold Eq. (17) without leaving the confinement region. The higher the initial pitch, the quicker the electron leaves the trap in the poloidal direction, see Figs. 12(b) and 12(c), so the higher the initial kinetic energy of this electron can be without it being lost. This allows electrons with higher initial kinetic energy to stay confined and explains the shape of $W_k^{sep}(\lambda)$.

If the electron is detrapped with a positive pitch, as in Fig. 12(b) it continues its motion in the positive θ direction. It is quickly helically retrapped and subject again to large drifts in the radial direction, thus increasing its chances of leaving the confinement region. That is the case for electrons having an initial pitch $0.25 \lesssim |\lambda| \lesssim 0.5$ in Fig. 11. However if an electron is detrapped with a negative pitch, as in Fig. 12(c), its rotation changes to the negative θ direction and the

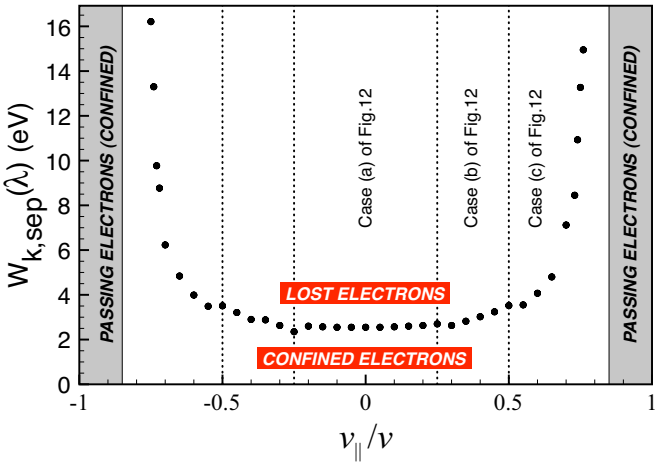

FIG. 11. (Color online) Separatrix between confined and lost electrons from Fig. 10 above, in (λ, W_k) space. The three regions described in the discussion are highlighted here. The estimate Eq. (17) gives a threshold kinetic energy $W_k^{sep}(0)=2.88$ eV, in rough agreement with the value of 2.55 eV found numerically here.

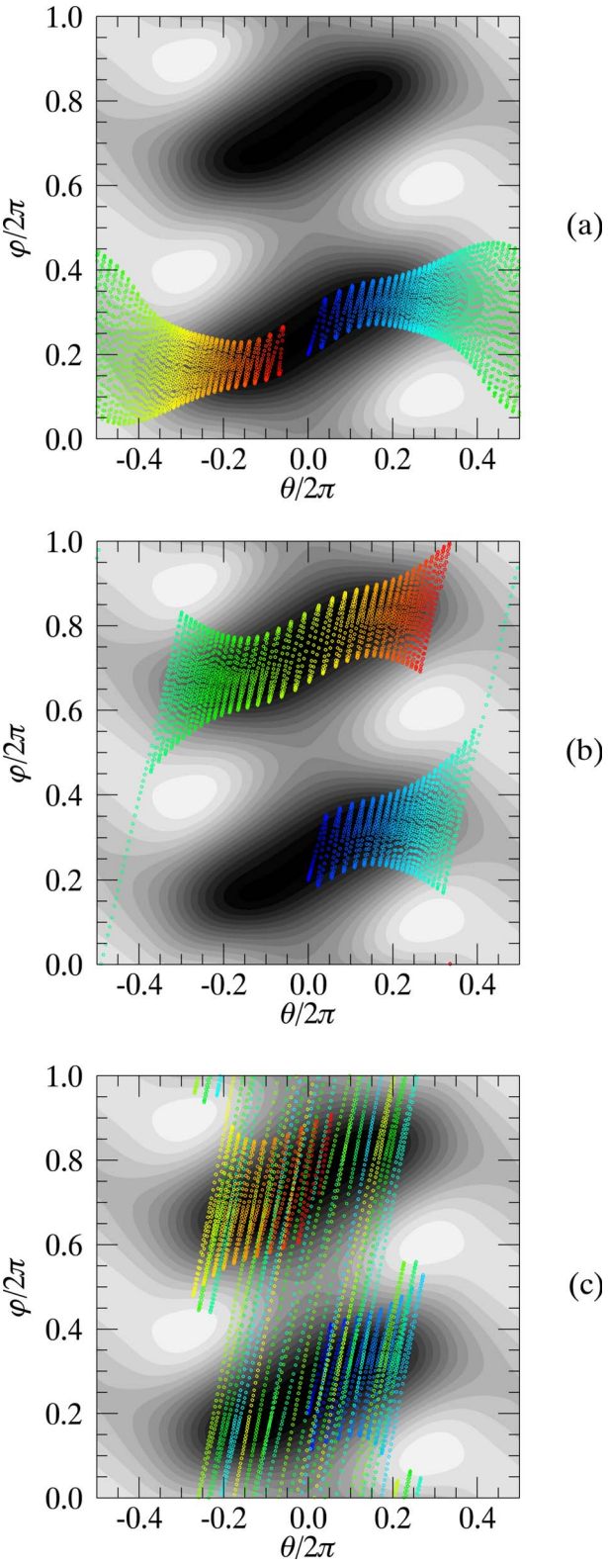

FIG. 12. (Color online) Changes in the orbit of a 2 eV electron with initial pitch: (a) $\lambda=0.2$, (b) $\lambda=0.45$, and (c) $\lambda=0.7$. The orbit is superimposed over a contour plot of the magnetic field strength on the surface $\psi/\psi_b=0.9$.

electron become toroidally trapped for some time, thus drastically reducing its radial excursion and its chances to leave the confinement region. That is the case for electrons having $0.5 \lesssim |\lambda|$ in Fig. 11.

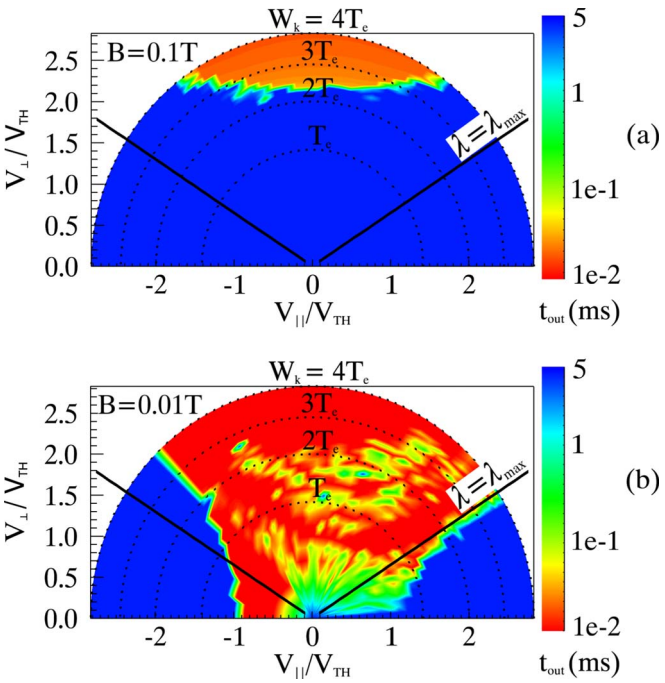

FIG. 13. (Color online) Deterioration of the loss cone by resonant electrons in the case of a strong and purely radial electric field. (a) $B=0.1$ T is far from resonance. (b) $B=0.01$ T and the resonance appears clearly as a fraction of counterpassing electrons is lost. These loss cones are at a minimum of B on the surface $\psi=0.7\psi_b$.

C. Resonances

$\vec{E}\times\vec{B}$ rotation is in the positive θ direction. So this rotation *adds* to the ι-induced poloidal rotation for copassing electrons ($\lambda>0$) whereas it *subtracts* from the ι-induced poloidal rotation for counterpassing electrons ($\lambda<0$). For very strong electric fields these two rotations can cancel out for counterpassing particles leading to a *toroidal resonance*.[26] The $\vec{E}\times\vec{B}$ velocity is

$$v_{\vec{E}\times\vec{B}} = \frac{E}{B} \simeq \frac{\Delta\Phi}{aB} \tag{18}$$

and the ι-induced velocity is

$$v_\iota = v_\parallel \frac{B_\theta}{B} \simeq \epsilon\iota v_\parallel, \tag{19}$$

where ϵ is the inverse aspect ratio $\epsilon \equiv a/R$. Estimating $\Delta\Phi$ with Poisson's equation and $v_\parallel \simeq v_{th} \equiv \sqrt{T/m}$ yields the approximate resonance condition,

$$N_D^2 \rho_L \simeq \iota\epsilon a, \tag{20}$$

where $N_D = a/\lambda_D$ is the number of Debye lengths in the plasma and ρ_L is the electron Larmor radius. The resonance condition can be fulfilled for typical conditions of operation in CNT. For the potential we have chosen here, a resonance is observed with $B \sim 0.02$ T, which is a typical magnetic field in CNT. Resonances deteriorate confinement because resonant electrons stay localized at a fixed poloidal location. Resonances affect most highly counterpassing electrons ($\lambda \sim -1$) leading to the loss of these, see Fig. 13.

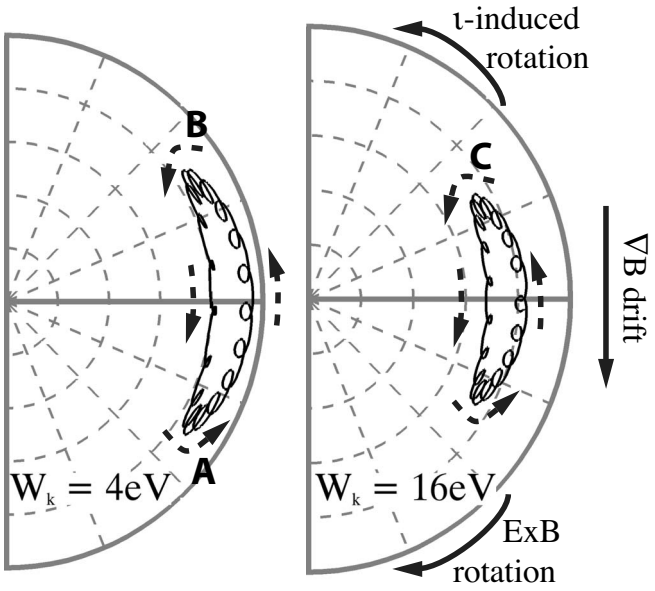

FIG. 14. Two "bananalike" orbits starting at the same initial location and with the same initial pitch ($\lambda=-1$). The only difference is the initial kinetic energy: 4 eV (left) and 16 eV (right).

An interesting class of orbits appears because of this toroidal resonance. In a cross sectional view these present themselves with a shape somewhat similar to that of banana orbits in tokamaks. However, these new orbits are very different: They occur for counterpassing particles only, and as mentioned, are due to a resonance between $\vec{E}\times\vec{B}$ induced poloidal rotation and ι-induced poloidal (counter-) rotation. Two representative examples are shown in Fig. 14 and a 3D view is given in Fig. 15.

The overall banana shape can be understood as follows, in reference to the left hand orbit on Fig. 14: An electron with negligible perpendicular kinetic energy and about 4 eV parallel kinetic energy has downward curvature magnetic drift. The $\vec{\nabla}B$ drift is in the same direction but is negligible. Starting at the midplane, the electron is initially rotating clockwise in the poloidal direction since its $\vec{E}\times\vec{B}$ motion (which is clockwise) dominates the ι-induced rotation. This rotation takes it down to a point where the magnetic drift (still down) now causes the electron to drift out to larger magnetic surfaces (higher ψ values). As the electron drifts radially to outer surfaces, its kinetic energy increases as its potential energy decreases; because of μ conservation and the small value of μ, the vast majority of that energy goes into the parallel motion. Since the electron now moves faster along B, its ι-induced poloidal rotation rate increases, and the net poloidal rotation rate slows down and eventually reverses. At the reversal point, the electron is at the bottom of the banana orbit (*label A*). The electron is still drifting to larger magnetic surfaces, thus still increasing its parallel kinetic energy because of the electrostatic potential energy drop. The poloidal rotation of the electron is now counterclockwise; it is in the direction of the ι-induced rotation. It will continue on this path to the upper part of the plot, where the downward magnetic drifts begin to bring the particle inward, to inner magnetic surfaces, and higher electrostatic potential energy. Hence, the electron loses parallel energy, decreasing and eventually reversing the net poloidal rotation rate to the $\vec{E}\times\vec{B}$ drift direction (clockwise), at the top of the banana (*label B*), and returns, essentially closing its orbit.

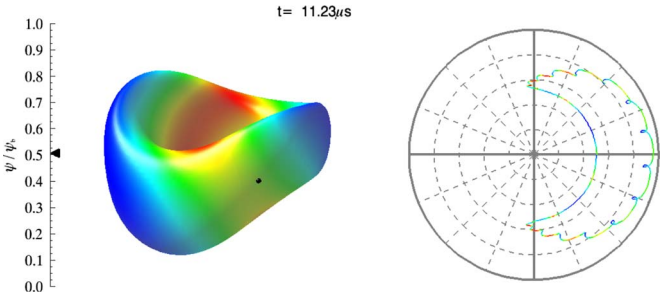

FIG. 15. (Color online) "Bananalike" orbit of a resonant electron. On the left hand side is a vertical scale giving ψ/ψ_b, the normalized radial position of the electron. In the middle is a 3D view of the electron on its magnetic surface. The surface is colored according to the magnitude of $\vec{B}$ on this surface, red being high B, yellow-green being mild B, and blue being low B. On the right hand side is the trajectory of the electron projected onto the (ψ,θ) plane (enhanced online).[URL: http://dx.doi.org/10.1063/1.3259967.3]

If the electron is instead initialized at the same point, but with 16 eV of almost exclusively parallel kinetic energy (right hand side of Fig. 14), it will begin by poloidally rotating in the counterclockwise direction (dominated by the ι-induced rotation), rotating into the upper region where the $\vec{\nabla}B$ drift is taking it inward. The inward drift reduces the parallel kinetic energy and ι-induced counterclockwise rotation to the point of reversal (*label C*), and one recognizes that its orbit is very similar, it just started on the outer part of the banana orbit instead of the inner part.

The much smaller loops that are seen in addition to the overall motion are caused by the toroidal variations of the $\vec{E}\times\vec{B}$ drift as the particle passes through the thin and the thick cross sections of CNT. In the two thick cross sections of CNT, both the electric and the magnetic fields are larger than in the two thin cross sections. However, the electric field does not increase as much as the magnetic field (it increases roughly as $1/a$, whereas the magnetic field increases as $1/a^2$, with a being the minor radius) so the $\vec{E}\times\vec{B}$ drift is smaller in the thin cross sections. Since the electron is resonant (ι-induced poloidal rotation and $\vec{E}\times\vec{B}$-induced rotation nearly canceling each other), the poloidal rotation is in one direction in the two thin cross sections and in the opposite direction in the two thick cross sections, giving rise to two small loops for each toroidal rotation of the electron—two because CNT is a two-period stellarator.

We must emphasize the fact that although they look similar, these "bananalike" orbits are very different from the ones found in tokamaks. In tokamaks, banana orbits are due to toroidicity and the direction of the shift from the flux surface depends on the sign of the initial parallel velocity of the particle. Here "bananalike" orbits are due to resonances in the poloidal motion, occurring for counterpassing electrons only, and the direction of the shift depends on the initial parallel kinetic energy of the electron. Indeed if the electron is born with little parallel kinetic energy, its initial poloidal

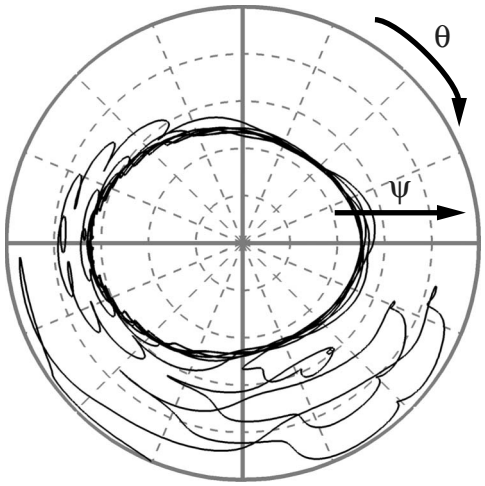

FIG. 16. Complicated trajectory of an electron in the real potential of CNT, nonconstant on magnetic surfaces. The electron born at $\psi=0.5\psi_b$ with 4 eV kinetic energy ends up being lost.

motion is in the positive θ direction. If it is born with a lot of parallel kinetic energy its initial poloidal motion is in the negative θ direction.

V. POTENTIAL NONCONSTANT ON SURFACES

We now turn to the most relevant case to CNT: an electrostatic potential that depends on all three spatial coordinates. Variations in the electric potential in the poloidal direction create radial $\vec{E}\times\vec{B}$ drift. This drift does not depend on the kinetic energy of the electron as magnetic drifts do. Even low energy electrons can make significant radial excursions. Moreover by doing so, they can pick up kinetic energy from the electric field and effectively increase their magnetic drifts.

The combination of all these effects makes analytical calculation impractical. The complexity of the trajectories is illustrated in Fig. 16 (Fig. 17), where we plot the trajectory

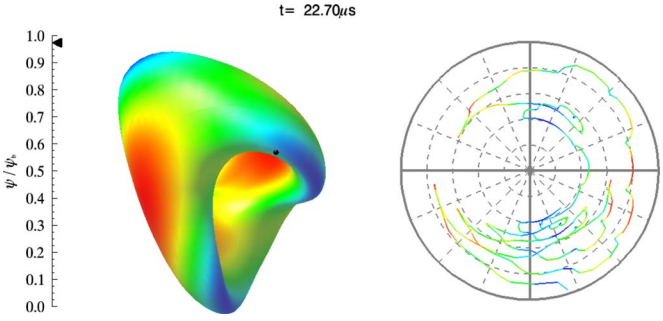

FIG. 17. (Color online) Trajectory of an electron in a potential nonconstant on magnetic surfaces. On the left hand side is a vertical scale giving ψ/ψ_b, the normalized radial position of the electron. In the middle is a 3D view of the electron on its magnetic surface. The surface is colored according to the effective potential $\mu B - e\Phi$ on this surface—see Eq. (21). Red is high potential, yellow-green is mild potential, and blue is low potential. On the right hand side is the trajectory of the electron projected onto the (ψ,θ) plane (enhanced online).[URL: http://dx.doi.org/10.1063/1.3259967.4]

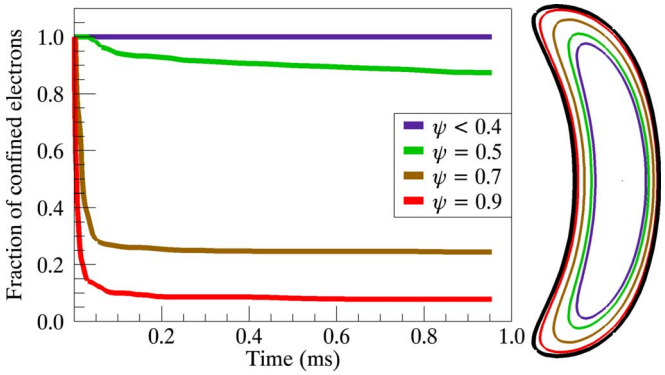

FIG. 18. (Color online) Fraction of confined electrons in the case of an electric potential with significant variations on surfaces. 1000 4 eV electrons are started on each surface. Losses are significant even deep in the plasma.

of the same electron as in Figs. 2 and 6 (Figs. 3 and 7) but in a potential $\Phi(\psi,\theta,\phi)$ typical of CNT before the installation of conducting boundaries.

Numerical integration of the trajectories of 4 eV electrons started on different surfaces shows that there exists a large fraction of unconfined orbits even deep inside the plasma, see Fig. 18. Intuitively this is understood as follows. Without electric field and neglecting magnetic drifts, electrons circulate all around magnetic surfaces following field lines. Now if there is an electric field, electrons also $\vec{E}\times\vec{B}$ drift on equipotential surfaces because $\vec{v}_{\vec{E}\times\vec{B}}=\vec{E}\times\vec{B}/B^2=-\vec{\nabla}\Phi\times B/B^2$ so that $\vec{v}_{\vec{E}\times\vec{B}}\cdot\vec{\nabla}\Phi=0$. Moreover if the equipotential surfaces do not match magnetic surfaces, electrons can jump from one magnetic surface to the other. After a few steps of jumping from one surface to the other an electron can find its way out of the plasma, see Fig. 19. Simulations show that this process is quite effective and can remove electrons from the plasma in tenths of microseconds, see Fig. 18.

The complexity of the trajectories in this potential is well illustrated by the complexity of the loss cone in velocity space, see Fig. 20. In particular, one does not observe any threshold energy for electrons to leave confinement as is the case for $\Phi(\psi)$. As explained before, this is because now $\vec{E}\times\vec{B}$ drift, which does not depend on kinetic energy, can bring

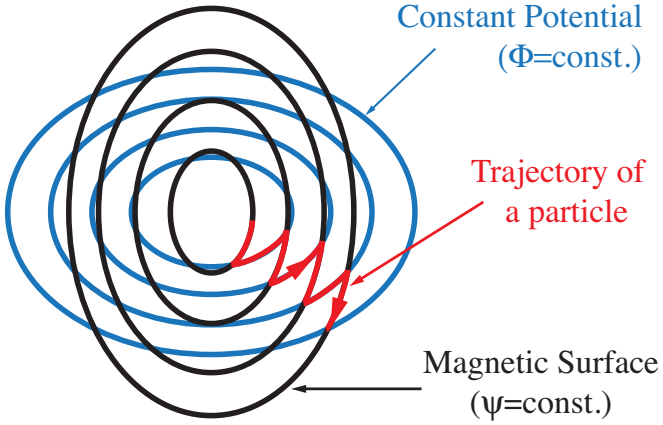

FIG. 19. (Color online) Conceptual sketch of mismatch loss process. Electrons jump from magnetic surface to magnetic surface by drifting on equipotentials and magnetic surfaces and can find their way out of the plasma.

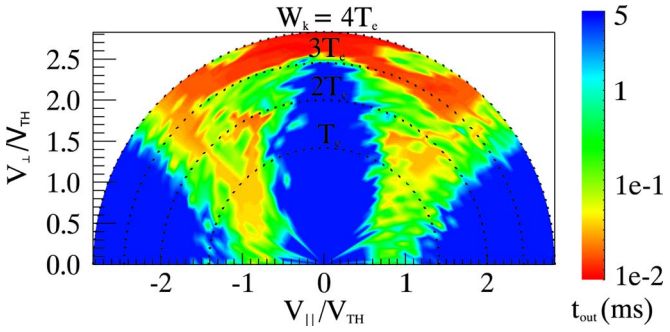

FIG. 20. (Color online) Complicated loss cone structure in the case of an electric potential significantly varying on surfaces, typical of CNT. t_{out} denotes the time it takes an electron to leave confinement. A 5 ms confinement time is considered infinite confinement time.

electrons past the last closed magnetic surface. The good confinement regions of Fig. 20 can be explained by looking at the trapped-passing separatrix. Because the potential now varies on surfaces, this separatrix differs significantly from a straight line.[27] An electron born at a potential Φ_0 and magnetic field B_0 with velocity $(v_\parallel, v_\perp)$ moves in an effective potential $\mu B - e\Phi$ and is trapped on a magnetic surface if

$$(\mu B - e\Phi)_{\max} > \tfrac{1}{2} m_e (v_\parallel^2 + v_\perp^2) - e\Phi_0, \tag{21}$$

where the subscript max stands for maximum on the magnetic surface. In particular, for an electron born with $|\lambda| = 1$, this inequality reduces to

$$|v_\parallel| < \sqrt{\frac{2e(\Phi - \Phi_{\min})}{T_e}}\, v_{\text{th}}. \tag{22}$$

So the good confinement regions on the sides are associated with electrons being barely trapped and thus being confined by $\vec{E} \times \vec{B}$ rotation. The good confinement region near $\lambda \sim 0$ comes from the fact that $\lambda = 0$ particles are deeply trapped and just drift on the equipotential contours. Deep inside the plasma these contours close on themselves and the electrons can never cross the separatrix.

VI. CONCLUSION

The strong radial electric field created by charge imbalance in CNT has been shown to greatly improve the orbits, as expected. However two main mechanisms have been identified that can create unconfined trajectories in CNT despite this large radial electric field. First, even when the electric potential is perfectly constant on surfaces, toroidal resonances occur that destroy orbits confinement. Second, nonconstancy of the electric potential on surfaces also create unconfined trajectories. The electric potential used in Sec. V is the potential in CNT with electrostatic boundary conditions imposed by the coils and the vacuum chamber. The recent installation of a conducting boundary surrounding the plasma should then improve considerably the trajectories. Indeed even if it does not make the potential perfectly constant on surfaces, it certainly greatly reduces its variations on surfaces. More work is underway to characterize more precisely how the potential at the plasma boundary is affecting the trajectories and transport in CNT.

ACKNOWLEDGMENTS

This work was supported by the NSF-DOE under Grant No. NSF-PHY-06-13662.

[1] J. H. Malmberg and J. deGrassie, Phys. Rev. Lett. **35**, 577 (1975).
[2] T. O'Neil, Phys. Fluids **23**, 2216 (1980).
[3] D. E. Eggleston, K. J. McMurtry, A. A. Kabantsev, and C. F. Driscoll, Phys. Plasmas **13**, 032303 (2006).
[4] D. H. E. Dubin, Phys. Plasmas **15**, 072112 (2008).
[5] A. A. Kabantsev and C. F. Driscoll, Phys. Rev. Lett. **89**, 245001 (2002).
[6] A. A. Kabantsev and C. F. Driscoll, Fusion Sci. Technol. **47**, 263 (2005).
[7] E. M. Hollmann, F. Anderegg, and C. F. Driscoll, Phys. Plasmas **7**, 2776 (2000).
[8] J. Danielson, C. Surko, and T. O'Neil, Phys. Rev. Lett. **99**, 135005 (2007).
[9] R. C. Davidson, *Physics of Nonneutral Plasmas* (Imperial College Press, 2001).
[10] K. Avinash, Phys. Fluids B **3**, 3226 (1991).
[11] N. Crooks and T. O'Neil, Phys. Plasmas **3**, 2533 (1996).
[12] J. Marler and M. Stoneking, Phys. Rev. Lett. **100**, 155001 (2008).
[13] M. Stoneking, J. Marler, B. Ha, and J. Smoniewski, Phys. Plasmas **16**, 055708 (2009).
[14] T. S. Pedersen and A. H. Boozer, Phys. Rev. Lett. **88**, 205002 (2002).
[15] T. S. Pedersen, A. H. Boozer, J. P. Kremer, R. G. Lefrancois, W. T. Reiersen, F. Dahlgren, and N. Pomphrey, Fusion Sci. Technol. **46**, 200 (2004).
[16] T. Sunn Pedersen, J. P. Kremer, R. G. Lefrancois, Q. Marksteiner, N. Pomphrey, W. Reiersen, F. Dahlgren, and X. Sarasola, Fusion Sci. Technol. **50**, 372 (2006).
[17] J. W. Berkery and A. H. Boozer, Phys. Plasmas **14**, 104503 (2007).
[18] J. W. Berkery, T. Sunn Pedersen, J. P. Kremer, Q. R. Marksteiner, R. G. Lefrancois, M. S. Hahn, and P. W. Brenner, Phys. Plasmas **14**, 062503 (2007).
[19] R. G. Lefrancois, T. Sunn Pedersen, A. H. Boozer, and J. P. Kremer, Phys. Plasmas **12**, 072105 (2005).
[20] H. E. Mynick, Phys. Fluids **26**, 2609 (1983).
[21] H. E. Mynick, Phys. Plasmas **13**, 058102 (2006).
[22] A. H. Boozer, Phys. Fluids **24**, 1999 (1981).
[23] G. Kuo-Petravic, A. H. Boozer, J. A. Rome, and R. H. Fowler, J. Comput. Phys. **51**, 261 (1983).
[24] A. H. Boozer and G. Kuo-Petravic, Phys. Fluids **24**, 851 (1981).
[25] G. Grieger, W. Lotz, P. Merkel, J. Nührenberg, J. Sapper, E. Strumberger, H. Wobig, the W7-X Team, R. Burhenn, V. Erckmann, U. Gasparino, L. Giannone, H. J. Hartfuss, R. Jaenicke, G. Kühner, H. Ringler, A. Weller, and F. Wagner, Phys. Fluids B **4**, 2081 (1992).
[26] U. Stroth, *Transport in Toroidal Plasmas*, Lecture Notes in Physics Vol. 670 (Springer, Berlin, 2005).
[27] J. Fajans, Phys. Plasmas **10**, 1209 (2003).